Journal of Solid State Chemistry **167,** 508–516 (2002)
doi:10.1006/jssc.2002.9669

Trivalent Cation Substitution Effect into Layered Double Hydroxides $Co_2Fe_yAl_{1-y}(OH)_6Cl \cdot nH_2O$: Study of the Local Order

Ionic Conductivity and Magnetic Properties

Mourad Intissar,* Rachid Segni,* Christophe Payen,† Jean-Pierre Besse,* and Fabrice Leroux*,[1]

*Laboratoire des Matériaux Inorganiques, CNRS-ESA no: 6002, Université Blaise Pascal, 63177 Aubière cédex, France; and †Institut des Matériaux Jean Rouxel, 2 rue de la Houssinière, BP 32229, 44322 Nantes cédex 03, France

Received February 25, 2002; in revised form May 13, 2002; accepted May 28, 2002

A series of layered double hydroxide materials of composition $Co_2Fe_yAl_{1-y}(OH)_6Cl \cdot nH_2O$ ($0 \le y \le 1$) was prepared via chimie douce. The crystalline parameter related to the cation to cation distance obeys the expected variation, showing that the substitution is effective over the entire range. Local order around Co and Fe cations is studied by X-ray absorption spectroscopy. Moduli of the Fourier transform at the Fe K-edge are superimposable, in agreement with an ordered model, although present in small domains since no superlattice is depicted. The ionic resistivity of the samples is highly dependent on the water molecule content. The conductivity is found to be thermally assisted, and the variation of the slope in the Arrhenius diagram is explained by a Vogel–Tamman–Fulcher-type behavior. Magnetic susceptibility measurements support the proposed cation composition and indicate the onset of local magnetic order at low temperature (below 10 K). The inter-sheet distance influences the magnetic response at low temperature, showing the presence of weak interactions between lamellae. © 2002 Elsevier Science (USA)

Key Words: **layered double hydroxides; intralamellar cation substitution; XRD and XAS techniques; complex impedance spectroscopy; magnetic properties.**

INTRODUCTION

Layered double hydroxide (LDH) materials are described with the general formula $M^{II}_{1-x}M^{III}_x(OH)^{x+}_2A^{z-}_{x/z} \cdot nH_2O$ (noted as $\left[M^{II}_rM^{III}-A\right]$, with $r = 1/x - 1$), in which the substitution of a portion of the divalent cations by trivalent cations gives rise to a net positive charge. This excess of charge is counterbalanced with anions present in the interlamellar region. LDH materials are ideally described by hydrotalcite, a natural anionic clay of the composition $Mg_2Al(OH)_6(CO^{2-}_3)_{0.5} \cdot 2H_2O$ (1). LDH materials have been extensively studied in terms of thermal evolution (2–5), textural properties (6–7), formation of nanosized metal particles (8, 9) or environmental purpose (10). LDH calcined products are finding applications in catalysis (11). For such a purpose, a well-dispersed arrangement of the active centers is desirable. Therefore, a corresponding cationic ordering is preferred within LDH sheets (12). In the literature, some LDH systems that possess cation ordering are $Li_2Al(OH)_6Cl \cdot 2H_2O$ (13), [Mg_3Ga–carbonate] (14) and [Mg_2Al–benzoate or sulfate] (15).

The order may originate from

- the diffusion of one of the cations into open framework sites; this is exemplified by $Li_2Al(OH)_6Cl \cdot 2H_2O$ where Li^+ cations migrate into the octahedral sites that are $\frac{1}{3}$ vacant in the $Al(OH)_3$ bayerite structure,
- compatibility in the cation size such as in the [Mg_2Ga] system (12),
- a well-ordered packing of the interlayered anions, as occurs for benzoate or sulfate anions with [Mg_2Al] LDH matrix.

In this study, focus is on [$Co_2Fe_{1-y}Al_y$–Cl] ($0 \le y \le 1$) LDH materials. One question to address is the effect of the substitution on the local order. Previous studies demonstrate that, in spite of the lack of a superlattice, a pronounced local order was observed for [Co_2Al–Cl] (16). The pyroaurite-type compound (PTC) [Co_2Fe–CO_3] is also well crystallized (17). X-ray absorption spectroscopy (XAS) is utilized because it is known to provide powerful means for assessing the degree of cation ordering in LDH materials on a local scale (18–21). The magnetic properties may also shed some light on both the electronic and structural features (22). Thus, we have measured the magnetic susceptibility of the substituted samples and of the dodecylsulfate exchanged derivatives. Surfactant

[1]To whom correspondence should be addressed. E-mail: fleroux@chimtp-univ.bpclermont.fr.

0022-4596/02 $35.00

molecules prop the layers of the pristine material. The magnetic properties are then compared to address whether the interlayer interactions have a significant effect. In addition, complex impedance measurements were performed to evaluate the influence of the substitution on the mobility of charge carriers.

EXPERIMENTAL

Preparation of the Samples

Metal chlorides $CoCl_2 \cdot 6H_2O$ (98%, Aldrich), $FeCl_3 \cdot 6H_2O$ (98%, Prolabo), $AlCl_3 \cdot 6H_2O$ (99%, Acros), sodium dodecylsulfate $C_{12}H_{25}SO_4Na$ (noted as DS, 98%, Prolabo) and sodium hydroxide NaOH (Aldrich) were used as received. $Co_2Fe_{1-y}Al_y(OH)_2Cl \cdot nH_2O$ LDH materials (noted as [$Co_2Fe_{1-y}Al_y$–Cl]) were prepared by coprecipitation at a constant pH of 10.5, as described by Miyata (23). The synthesis was performed at room temperature with decarbonated water under nitrogen atmosphere to minimize carbonate anion contamination. Exchange with DS solutions was carried out using twice the amount corresponding to the LDH exchange capacity ranging from 1.7 to 2.25 meq g^{-1}. Chemical analyses were performed using inductive conduction plasma coupled to atomic emission spectroscopy (ICP/AES) at the Center of Analysis of CNRS (Vernaison, France).

Techniques of Characterization

X-ray diffraction. Powder X-ray diffraction (PXRD) patterns were obtained with a Siemens D500 X-ray diffractometer using Cu$K\alpha$ radiation The samples were scanned from 2° to 76° (2θ) in steps of 0.06 with a counting time of 4 s.

X-ray absorption spectroscopy — Co and Fe K-edge: X-ray absorption fine structure (XAFS) studies were performed at LURE (Orsay, France) using X-ray synchrotron radiation emitted by the DCI storage ring (1.85 GeV positrons, average intensity of 250 mA) at the D44 line. Data were collected at room temperature in transmission mode at the Fe and Co K-edge (7112.0 and 7708.9 eV, respectively). A double-crystal Si (1 1 1) monochromator scanned the energy in 2 eV steps from 100 eV below to 900 eV above the absorption edge. Three spectra were recorded for each sample with an accumulation time of 2 s per point. EXAFS spectra were evaluated by the classical plane-wave single scattering approximation, as previously described (24). The resultant $\chi(k)$ signal was fitted by using the formula $\chi(k) = S_0^2 \sum A_i(k) \sin[2kr_i + \phi_i(k)]$, with the amplitude $A_i(k) = (N_i/kr_i^2)F(k)\exp(-2k^2\sigma_i^2)$, where r_i is the interatomic distance, ϕ_i the total phase shift of the ith shell, N_i the effective coordination number, σ_i the Debye–Waller factor, and $F_i(k)$ the backscattering amplitude. EXAFS signal treatments and refinements were performed using available program package (25). The commonly accepted fitting accuracy is about 0.02 Å for the distance and 15–20% for the number of neighboring atoms.

Magnetic measurements. Magnetic measurements were performed on a commercial SQUID magnetometer. The magnetization M was first measured as a function of the field at $T = 150$ K in order to verify if there was any evidence for ferromagnetic impurity. The magnetic susceptibility, $\chi = M/H$, was measured with an applied field H of 100 and 1000 Oe in the 2–300 K temperature range. The samples were first cooled down to 2 K in the absence of field and then measured upon warming up to 300 K in an applied static field. All data were corrected for the effects of the sample holder and for core diamagnetism by using Pascal's constants (26).

Conductivity. Materials were equilibrated in a 60% RH atmosphere. Cylindrical pellets of 10 mm diameter and 1.9 mm thickness were prepared by cold pressing at 750 MPa. The material is sandwiched between graphite electrodes and placed into an air-tight cell. Conductivity measurements were performed by the complex impedance method carried out with a frequency analyzer (Solartron 1174). The frequency range was from 1 to 10^6 Hz, and the temperature cycle was between −20°C and 85°C. The "RKQ" (R and K in parallel with Q in series) model developed by Casciola *et al.* was applied to simulate the impedance spectra (27). After removal of the geometric capacitance of the cell, the impedance plots were refined by the expression

$$Z = (RZ_k/(R + Z_k)) + Z_Q, \qquad [1]$$

K and Q are constant phase angle elements, related to dielectric relaxation in the material and electrode phenomena, respectively, and expressed as $Z_k = K^{-1}(j\omega)^{-n}$ and $Z_Q = Q^{-1}(j\omega)^{-p}$ $(0 \leq (n, p) \leq 1)$.

RESULTS AND DISCUSSION

Chemical Analysis

The chemical formulae reported in Table 1 as a function of Fe^{III} to Al^{III} substitution are following the initial cation ratio used in the preparation. This indicates that the coprecipitation was complete for all the values of y. A contamination with carbonate ions is observed, representing as much as ≈10% of the anions, due to the great affinity of the LDH surface toward carbonate anions (28).

X-Ray Diffraction

X-ray diffraction patterns, displayed in Fig. 1, present features consistent for LDH materials. The structure is commonly described with a hexagonal lattice using

TABLE 1
Chemical and Structural Informations for $[Co_2Al_{1-y}Fe_y–Cl]$ LDH Samples

y	$(Co/M^{III})_{exp}$	$(Fe/Al)_{exp}$	Chemical composition	a (Å)	c (Å)	L_c (Å)[a]
0	2.18	0	$Co_{0.66}Al_{0.31}(OH)_2Cl_{0.25}(CO_3)_{0.04}\cdot 0.62H_2O$	3.05	22.91	430
0.25	2.103	0.36	$Co_{0.68}Fe_{0.08}Al_{0.23}(OH)_2Cl_{0.23}(CO_3)_{0.05}\cdot 0.23\ H_2O$	3.06	23.14	380
0.50	2.08	1.11	$Co_{0.66}Fe_{0.17}Al_{0.15}(OH)_2Cl_{0.25}(CO_3)_{0.04}\cdot 0.74\ H_2O$	3.07	23.27	370
0.75	2.09	3.17	$Co_{0.66}Fe_{0.25}Al_{0.08})(OH)_2Cl_{0.205}(CO_3)_{0.06}\cdot 0.64\ H_2O$	3.09	23.52	345
1	1.96	—	$Co_{0.66}Fe_{0.34}(OH)_2Cl_{0.183}(CO_3)_{0.07}\cdot 0.43\ H_2O$	3.11	23.68	420

[a] L_c (Å) is defined as the coherence length for the stacking direction estimated from the (006) *fwhm* using the Scherrer formula: $D_{hkl} = K\lambda/\beta_{1/2}\cos\theta$, where λ is the X-ray wavelength, θ the diffraction angle, $\beta_{1/2}$ the width at half-maximum intensity and K, a constant usually taken equal to 0.9.

rhombohedral symmetry with only $-h+k+l=3n$ reflections. Comparatively, $[Co_2Al–Cl]$ presents a better crystallinity than the other substituted materials, as shown by the (110) reflection. The incorporation of Fe^{III} cations induces an overlap of the two peaks (110) and (113). Parameters were refined by using $R\bar{3}\ m$ symmetry, and the values of ***a*** and ***c*** parameters are reported in Fig. 2. It appears that the lattice parameter ***a*** increases with the substitution, as expected with the difference of size between the two cations. This increase is linear, in agreement with Vegar's law (16). According to the ideal model of perfect edge-sharing octahedra, the variation of ***a*** with the substitution is expressed by the relation

$$\delta a/\delta yth = 0.33 * \sqrt{2}[r(Fe^{3+})] - r(Al^{3+})]. \qquad [2]$$

The linear dependence of ***a*** vs y is consistent with the variation of cation size (Fig. 2a), i.e., $\delta a/\delta_{th} = 0.061$(Å) and $\delta a/\delta y_{exp} = 0.062$(Å). This shows clearly that the substitution is taking place in the sheets.

The thickness of the brucite-like layer and of the interlayer distance is estimated from the c parameter. According to the stacking mode sequence ($3R$), ***c*** is related to three times the distance given by d_{003}. It is well established that the attractive forces between the positively

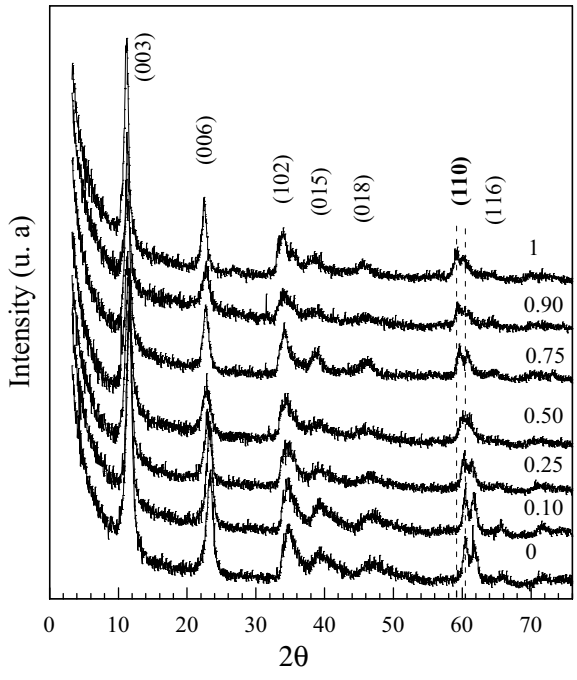

FIG. 1. Stacked plot of the XRD patterns of $[Co_2Fe_yAl_{1-y}–Cl]$ LDH samples. The substitution y is indicated. (110) peaks are shown with the dashed lines.

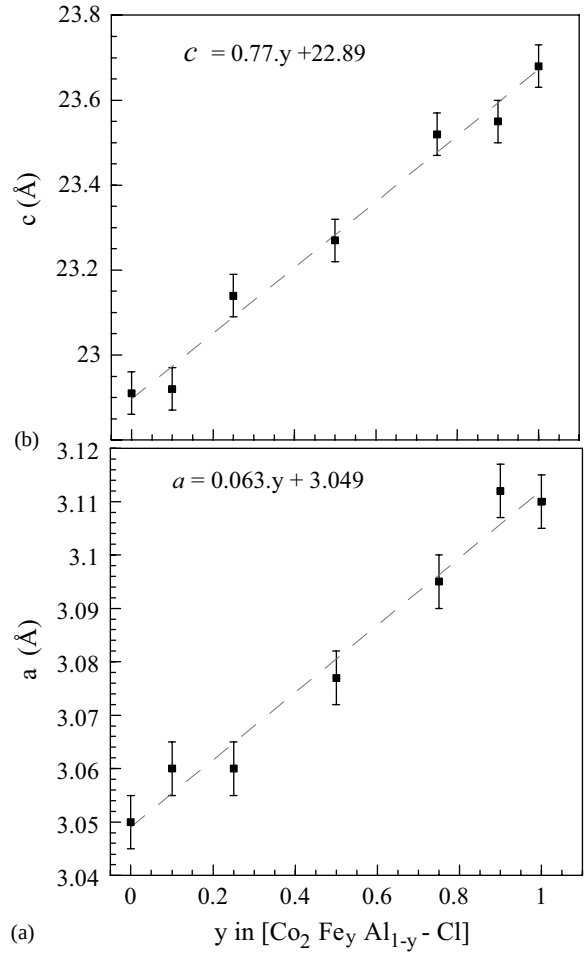

FIG. 2. Variation of parameters (a) ***a*** and (b) ***c*** vs y (Fe^{III} content) in $[Co_2Fe_yAl_{1-y}–Cl]$ LDH samples.

charged sheets and the interlayer anions are the main factors governing the variation of ***c***.

A change of the basal spacing is generally associated with a variation of the layer charge density, and an increase of trivalent cations induces a decrease of the basal spacing with more compensating anions present between the layers. However, the charge of the layer is kept constant for the title compounds, and a linear variation of ***c*** is observed (Fig. 2b). Since the variation of ***c*** is found to be linear across the range of substitution, independent of either the interlayer water molecule or carbonate anion content (Table 1), it must be explained by the substitution. Like other authors (29), we think that this induces an increase in the thickness of the layers. This situation is not observed for the $[(Co_{1-y}Cu_y)_2Al–Cl]$ LDH system, due to a structural transition from hydrotalcite to bottalackite upon substitution (30).

The coherence length was calculated from the half width of (003) lines using the Scherrer equation (Table 1). The coherent domain along the stacking direction is greater for the end-member materials $[Co_2Al–Cl]$ and $[Co_2Fe–Cl]$ than for the substituted samples. This parameter was found to be highly dependent on the nature of LDH materials (31).

XAS—Local Order Study

The moduli of the Fourier transform at Co and Fe K-edges are displayed in Fig. 3. The first peak is attributed to the shell of oxygen atoms surrounding the absorbing atom, the second to the metal to metal contribution. Contributions at further distances are also observed and discussed in the following text.

The first two coordination shells are refined, and Fig. 4 shows the quality of the fit for $[Co_2Al_{0.5}Fe_{0.5}–Cl]$. Cobalt cations are found to be in six-fold coordination (Table 2). The refined distance is consistent with the presence of Co^{II} cations. To estimate the relative amount of cations contributing to the metal–metal correlation, the number of backscattering atoms was free to move during the refinement. This guarantees all possible combinations between the cations for the second shell (16, 30, 32). The sum of backscattering atoms contributing to the second shell was found to be slightly overestimated, but kept within the uncertainty allowed by the EXAFS technique (Table 2). The aluminum cations are distinguished from the transition metals (Me = Fe, Co) by the amplitude and phase functions present at Co–Al distances shorter than for Co–*Me* (16). The similarity in electron scattering cross section and the phase shift between Fe and Co cations makes them indistinguishable by EXAFS. The Co–*Me* distance does not change with substitution (increase of y), whereas a shortening of the Co–Al distance is observed. The Debye–Waller factor, σ^2_{Co-Me}, is reduced in the absence of Fe^{III} cations, which seems to indicate that this

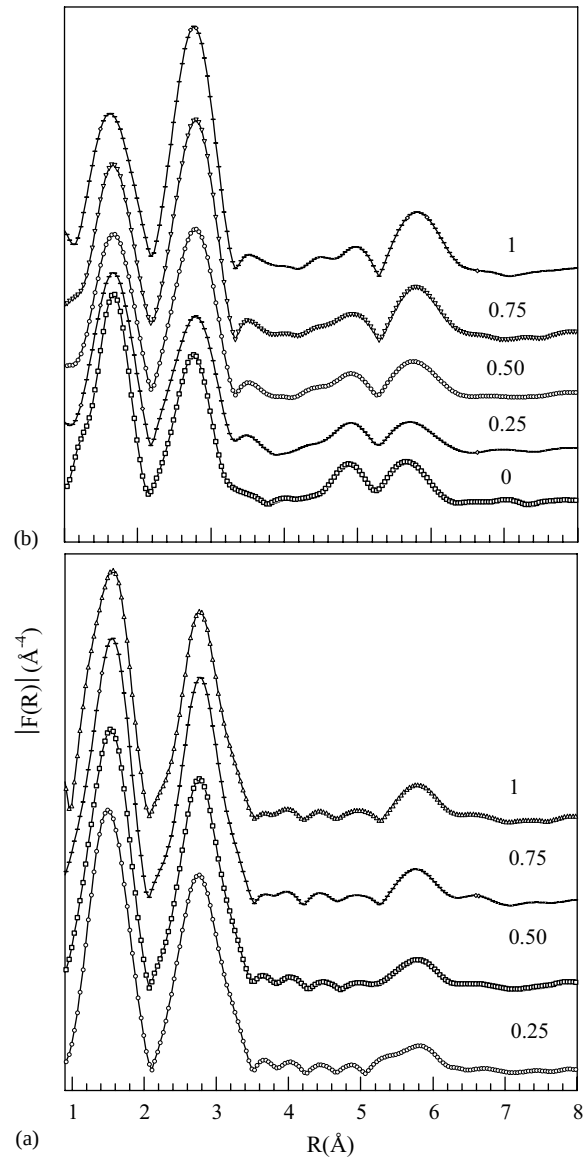

FIG. 3. Moduli of the Fourier transform of the EXAFS spectra at (a) Fe K-edge and (b) Co K-edge for $[Co_2Fe_yAl_{1-y}–Cl]$ LDH samples. The distances are not corrected for phase shift.

cation may be the origin of a greater disorder in the layer. This was also noticed in the X-ray diffraction patterns by the broadness of the (11*l*) lines (Fig. 1).

Concerning EXAFS Fe K-edge study, moduli of the Fourier transform present great similarities between each other. The Fe–O environment fits best six oxygen atoms at 2.02 Å (Table 2). The metal–metal correlation corresponds to either the presence of Fe or Co atoms (heavy backscatterer), and (Fe–Al) shell was needed for the refinement. The quality of the refinements is provided in Fig. 4. The results concerning Fe–*Me* is consistent with those obtained at the Co K-edge. The second peak intensity is unmodified with the substitution, whereas it increases in Fig. 3b. This

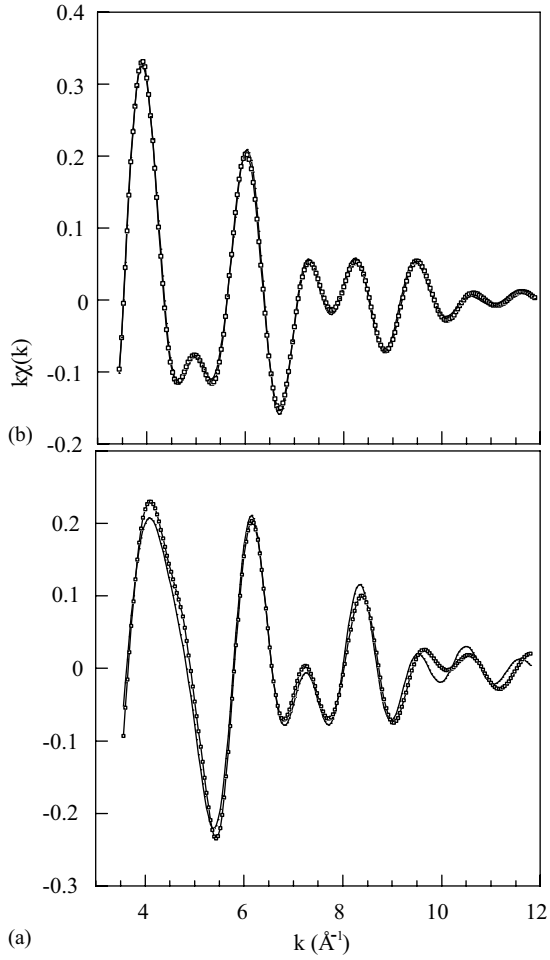

FIG. 4. Simulation of the first two shells for $[Co_2Fe_{0.5}Al_{0.5}–Cl]$ at (a) Fe K-edge and (b) Co K-edge.

let us surmise that Fe^{III} cations are surrounded only by divalent cobalt neighboring atoms, thus, supporting the idea of a cation order which is arising from a segregation of the trivalent cations. Such local order has been observed in PTCs such as $[Mg_2Fe–CO_3]$ (18). The cation ordering is also evidenced by the correlations arising from multiple scattering phenomena.

The XAS refinements can be interpreted and compared to the ideal cation arrangement supplied by an M^{II}/M^{III} LDH ratio of 2 to 1 (33). For the ideal approach, the divalent cations are surrounded by 3 M^{II} and 3 M^{III} at $2\boldsymbol{a}$ (as for the second shell of coordination) and only of M^{II} at $\boldsymbol{a}\sqrt{3}$, whereas 6 M^{III} and 6 M^{II} cations are present around trivalent cations at $\boldsymbol{a}\sqrt{3}$ and $2\boldsymbol{a}$, respectively. The latter is defined as the so-called focussing effect, sensitive to the angle between the three atoms lining up (34). The two contributions observed at the Co K-edge are either constant ($\boldsymbol{a}\sqrt{3}$) or dependent on the substitution ($2\boldsymbol{a}$), which is in agreement with the presence of an order around Co^{II} cations. At the Fe K-edge, the two contributions overlap (Fig. 3a). This shows that the order is not transmitted around Fe^{III} cations at longer ranges.

From XAS results, an average metal to metal distance may be calculated as

$$d_{Me-Me} = \tfrac{1}{3}[(1+2y)d_{Me-Me} + 2(1-y)d_{Me-Al}]. \quad [3]$$

The observed trend is in agreement with XRD results (Table 2), for $y = 0.75$, 0.50 and 0.25, $\langle d(Me-Me)\rangle$ $(= a) = 3.09$, 3.06 and 3.03 Å, respectively. This supports the idea of quasi-ordered domains. Nevertheless, the size of the domains remains small as the coherent picture is not visible by X-ray diffraction, probably on the order of a few tens of Å.

Magnetic Properties

Fig. 5 shows a χT vs T plot for all of the substituted materials in the $Co_2Fe_yAl_{1-y}(OH)_6 \cdot nH_20$ series. The $\chi(T)$ curves were obtained at a static applied field of 100 G. The effective moments at 300 K are given in Table 3. For $y = 0$, $[Co_2Al–Cl]$, the magnetic moment at 300 K is 5.1 B.M./Co atom, which is typical for octahedral high-spin ($S = \frac{3}{2}$) Co^{II} (35). In the high-temperature portion, χT values increase with the substitution of diamagnetic Al^{3+} by ($S = \frac{5}{2}$) Fe^{3+} cations. The room temperature magnetic moment is in agreement with the presence of Co^{II} and Fe^{III} in an octahedral environment and in proportion as defined by the nominal composition.

For all of the samples, a rapid increase of both χ and χT responses is observed below 20 K (Fig. 5), until they reach a maximum for a temperature on the order of $\approx$3–4 K.

For $y = 0$, this behavior is explained by the presence of intralayer ferromagnetic interactions between Co^{II} cations and the onset of a local intralayer ferromagnetic order. Comparatively, a sharp maximum in the $\chi(T)$ curve is observed for $Co(OH)_2$ at $T \approx 10$ K (36, 37). $Co(OH)_2$ presents a structural similarity with our sample, with the edge-sharing of $Co(OH)_6$ octahedra. With the incorporation of iron, one has to consider both ferromagnetic Co–Co and Co–Fe couplings. The decrease of χT between 60 and 30 K for the higher Fe^{III} content is consistent with the presence of antiferromagnetic Co–Fe coupling. Thus, a ferrimagnetic local order is expected to occur within the layers at low T, and this may be responsible for the peak in the susceptibility.

The long-range magnetic order for an ordered 2D system may also be due to interlayer dipolar coupling, as previously reported (37, 38). This prompted us to investigate the importance of such an effect in our samples. To do so, we studied the magnetic properties of DS derivative compounds, for which the surfactant molecule is propping the LDH sheets from 7.6 up to 25 Å (24). While the high-temperature response is unmodified by the DS incorporation, there are appreciable changes below 10 K (Fig. 6).

TABLE 2
Structural Parameters from EXAFS Refinement at Co and Fe K-edges for [$Co_2Al_{1-y}Fe_y$–Cl] LDH Samples

	Co K-edge					Fe K-edge				
y	Shell	N	R(Å)	$\sigma^2(10^{-3}Å^2)$	ρ(%)	Shell	N	R(Å)	$\sigma^2(10-3\,Å^2)$	ρ(%)[a]
0.0	O	6.3	2.06	6	1	—	—	—	—	—
	Co	3.8	3.12	8.1						
	Al	3.4	3.09	10						
0.25	O	6.2	2.08	7.22	3	O	6.5	2.02	5.62	4
	Me	5.5	3.13	14		*Me*	5.4	3.13	9.8	
	Al	1.4	2.92	5.47						
0.50	O	5.9	2.07	8.06	2	O	6.7	2.02	5.91	3
	Me	5.5	3.13	12.3		*Me*	5	3.13	10.2	
	Al	1.1	2.94	4.9						
0.75	O	6.2	2.07	7.2	4	O	6.7	2.01	5.97	3
	Me	6.0	3.13	10.2		*Me*	5.4	3.13	9.8	
	Al	1.1	2.95	6.9						
1.00	O	6.3	2.08	8.1	9	O	6.9	2.01	6.24	5
	Fe	6.7	3.14	10.4		Fe	5.7	3.14	11.4	

[a] Residual ρ factor is defined as $\rho = \sqrt{(\sum(k^3\chi_{exp}(k) - k^3\chi_{theo}(k))^2 / \sum(k^3\chi_{exp}(k))^2)}$.

This shows that interlayer interactions play a role at low temperature. The effect of the interlayer interaction depends on the intralayer couplings, as evidenced by the change in the modification. A greater χT response is observed for [Co_2Al–DS], whereas the opposite tendency appears for the [Co_2Fe–*DS*] LDH sample. In contrast, to well-defined layered systems (39), the magnetic properties are difficult to control by an expansion of the 2D character.

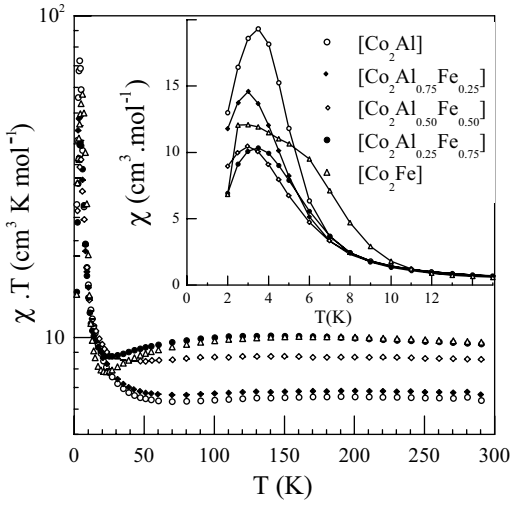

FIG. 5. $\chi(T)T$ vs T plot for [$Co_2Fe_yAl_{1-y}$–Cl] LDH samples in the range 2–300 K ($H = 100$ G). Inset:) $\chi(T)$ vs T plot in the temperature range 2–15 K ($H = 100$ G).

Conductivity

Since 2D open structures are suitable for ion mobility, the ionic conductivities of our samples were studied. Typical impedance plots (Cole–Cole plot) are shown for three compositions, $y = 0$, 0.5 and 1.0 in Fig. 7. Impedance spectra consist of an arc in the high frequency domain and a line inclined at 45° to the Z-axis in the low-frequency range (Fig. 7). The first feature disappears with an increase in temperature and is absent for [$Co_2Al_{0.50}Fe_{0.50}$–Cl].

The straight line is explained by the ion blocking effect (RQ in the circuit), and the semi-circle is affected mostly by

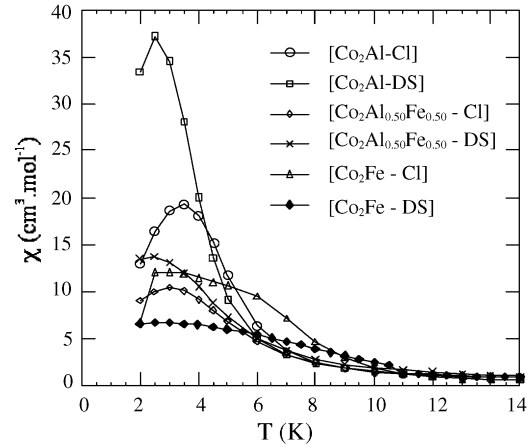

FIG. 6. Effect of the DS spacer molecule on the χ vs T response. y values are indicated.

TABLE 3
Results Obtained from Complex Impedance Spectroscopy (at 293 K) and from Magnetic Study for [$Co_2Al_{1-y}Fe_y$–Cl] LDH Samples

y	R (Ω)	K (10^{-9} S rd^{-n} s^n)	n	Q(10^3 Ω rd^p s^{-p})	p	χT at 293 K (cm^3 K mol^{-1})	μ_{eff}[a] at 293 K (B.M./fu)
1.0	578	3.9	0.70	8.6	0.56	9.64	8.8
0.75	413	4.1	0.71	5.4	0.55	9.51	8.7
0.50	72	—	0.160	3.44	0.57	8.48	8.2
0.25	933	2.0	0.78	8.9	0.55	6.80	7.4
0.0	1000	2.2	0.66	7.1	0.59	6.39	7.2

[a] μ_{eff} values are obtained from the relation $\mu_{eff}/\mu_B = 2.828\sqrt{(\chi T)}$.

the motion of the ions through and in between particle boundaries (RK). The elements K and Q correspond to the dielectric relaxation and electrode phenomena, respectively. K is of the order of a few nF, and capacitance of this magnitude (considering the modulus) is observed when the grain–boundary response is dominating the whole (40). The refinements of the impedance spectra are displayed in Table 3 for the data obtained at 20°C.

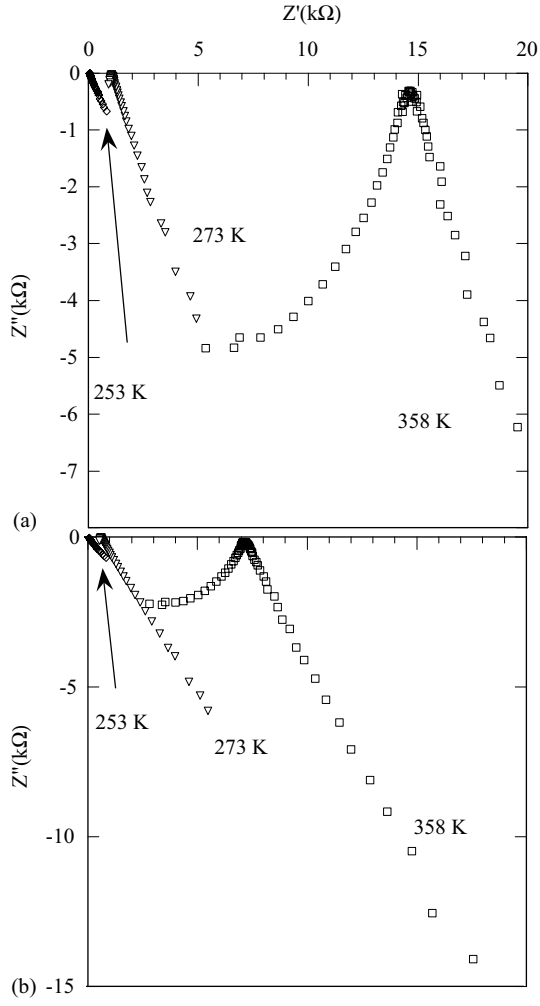

FIG. 7. [$Co_2Fe_yAl_{1-y}$–Cl] complex impedance spectra for (a) $y = 0$, and (b) $y = 1$.

All the conductivity data were fitted to the Arrhenius expression $\sigma = \sigma_0 \exp(-E_a/kT)$, where σ_0 is a pre-exponential factor, E_a the activation energy and k the Boltzmann constant. The data do not follow straightforwardly an Arrhenius law over the entire temperature range (Fig. 8). A slight deviation is noticed for temperatures higher than 325 K. Such behavior is explained on the basis of the conduction mechanism becoming thermally assisted, and expressed with a Vogel–Tamman–Fulcher (VTF)-type relationship (41). The values of E_a smaller than commonly observed for LDH materials (42) may be an indication of an ionic conductivity highly dependent on the hydration. This is illustrated in Fig. 9 with the variation of the resistivity (Table 3) as a function of the water molecules present in the materials. A quasi-linear behavior is fitted (Fig. 9). The conduction phenomenon has to be explained by the extrinsic water present at the surface of the crystallites, as stated earlier by de Roy and Besse (42).

Hysteresis is observed for $\log(\sigma T)$ vs $1/T$ when y is lower than 0.5. This occurs for other LDH materials such as [Zn_rAl–Cl] ($r > 2$) (43), and is explained by a chemical

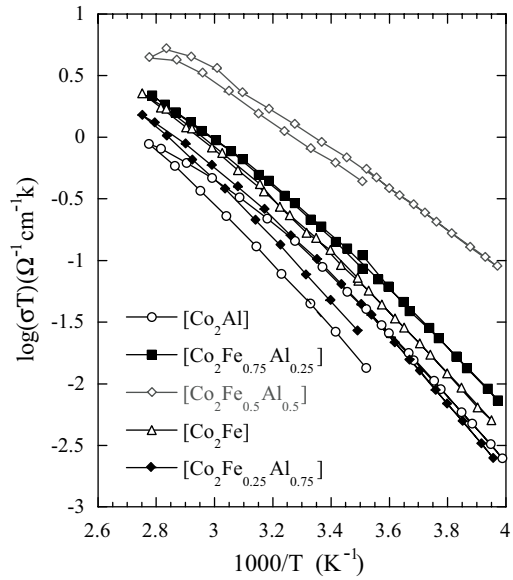

FIG. 8. Arrhenius-type plots for [$Co_2Fe_yAl_{1-y}$–Cl] LDH samples.

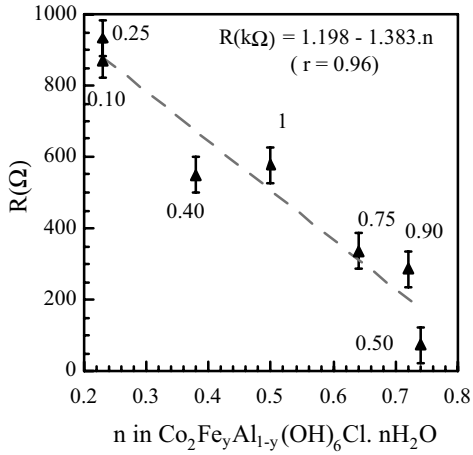

FIG. 9. Variation of the inverse of resistivity as a function of the number of water molecules. *y* values are indicated.

change during the experiment cycling at high temperature. The conductivity is comparable to that reported for other LDH materials (41, 42), and is much higher than that for 2:1 phyllosilicates such as montmorillonite clays (44).

CONCLUSION

This paper provides clear evidence of the incorporation of Fe trivalent cations inside [Co_2Al–Cl] LDH sheets over the entire range of substitution as shown by XAS results. The local order is supplied by the segregation surrounding the trivalent cations, i.e., no M^{III}–M^{III} correlation is present, but this prerequisite is not sufficient for the presence of order at long range. Moreover, the samples exhibit a weak interlayer dipolar coupling. The extrinsic water present at the surface of the crystallites plays an important role for the conduction phenomena. This study shows the importance of using a combination of characterization tools to better understand solids such as LDH materials.

ACKNOWLEDGMENTS

The authors thank Dr. S. Belin and V. Briois for their help in acquiring XAS spectra. We acknowledge the experimental opportunities at LURE (Orsay, France).

REFERENCES

1. R. Allman, *Chimia* **24,** 99 (1970).
2. M. Del Arco, P. Malet, R. Trujillano, and R. Rives, *Chem. Mater.* **11,** 624 (1999).
3. J. W. Boclair and P. S. Braterman, *Chem. Mater.* **11,** 298 (1999).
4. M. A. Aramendia, Y. Aviles, V. Boreau, J. M. Luque, J. M. Jose, J. R. Ruiz, and J. Francisco, *J. Mater. Chem.* **9,** 1603 (1999).
5. X. Hou and J. R. Kirkpatrick, *Inorg. Chem.* **40,** 6397 (2001).
6. F. Malherbe, C. Forano, and J.-P. Besse, *Microporous Mater.* **10,** 67 (1997).
7. G. Carja, R. Nakamura, T. Aida, and H. Niiyama, *Microporous Mesoporous Mater.* **47,** 275 (2001).
8. P. Beaudot, M. E. De Roy, and J.-P. Besse, *J. Solid State Chem.* **161,** 332 (2001).
9. K. A. Tarasov, V. P. Isupov, B. B. Bokhonov, Y. A. Gaponov, B. P. Tolochko, M. R. Sharafutdinov, and S. S. Shatskaya, *J. Mater. Synth. Process.* **8,** 21 (2000).
10. Y. Seida and Y. Nakano, *Water Res.* **34,** 1487 (2000).
11. A. de Roy, C. Forano, K. El Malki, and J.-P. Besse, *in* "Synthesis of Microporous Materials" (L. Ocelli and H. Robson, Eds.), Vol. 2, p. 108. Van Nostrand Reinhold, New York, 1992; A. Vaccari, *Catal. Today* **41,** 53 (1998).
12. M. Bellotto, M. Rebours, O. Clause, J. Lynch, D. Bazin, and E. Elkaïm, *J. Phys.Chem.* **100,** 8527 (1996).
13. J. P. Thiel, C. K. Chaing, and K. R. Poeppelmeir, *Chem. Mater.* **5,** 297 (1993).
14. A. Terzis, S. Filippakis, H. Kuzel, and H. Z. Burzlaff, *Kristallografiya* **29,** 181 (1987).
15. A. S. Bookin, V. I. Cherkashin, and J. A. Drits, *Clays Clay Miner.* **41,** 558 (1993); M. Vucelic, G. D. Moggridge, and W. Jones, *J. Phys. Chem.* **99,** 8328 (1995).
16. F. Leroux, El M. Moujahid, C. Taviot-Guého, and J.-P. Besse, *Solid State Sci.* **3,** 81 (2001).
17. H. C. B. Hansen, C. B. Koch, and R. M. Taylor, *J. Solid State Chem.* **113,** 46 (1994).
18. M. Vucelic, W. Jones, and G. D. Moggridge, *Clays Clay Miner.* **45,** 803 (1997).
19. H. Roussel, V. Briois, E. Elkaïm, A. de Roy, and J.-P. Besse, *J. Phys. Chem. B* **104,** 5915 (2000).
20. M. Köckerling, G. Geismar, G. Henkel, and H.-F. Nolting, *J. Chem. Soc., Faraday Trans.* **93,** 481 (1997).
21. I. Crespo, C. Barriga, M. A. Ulibarri, G. Gonzalez-Bandera, P. Malet, and V. Rives, *Chem. Mater.* **13,** 1518 (2001).
22. J. E. Greedan, *J. Mater. Chem.* **11,** 37 (2001); N. Hamanaka and H. Imoto, *Inorg. Chem.* **37,** 5844 (1998).
23. S. Miyata, *Clays Clay Miner.* 1975, **23,** 369.
24. F. Leroux, M. Adachi-Pagano, M. Intissar, S. Chauvière, C. Forano, and J.-P. Besse, *J. Mater. Chem.* **11,** 105 (2001).
25. Programs available on the web site of LURE, http.//www.lure.u-psud.fr.
26. "Landolt–Börstein Tables," Vol. I, Part 1, pp. 395–398. [Springer-Verlag, Berlin, 1950]
27. D. Bianchi and M. Casciola, *Solid State Ionics* **17,** 7 (1985).
28. J. Inacio, C. Taviot-Guého, C. Forano, and J.-P. Besse, *Appl. Clay Sci.* **18,** 255 (2001).
29. S. Velu, D. P. Sabde, N. Shah, and S. Sivasanker, *Chem. Mater.* **10,** 3451 (1998).
30. F. Leroux, El. M. Moujahid, H. Roussel, A.-M. Flank, V. Briois, and J.-P. Besse, *Clays Clay Miner.* **50,** 260 (2002).
31. C. O. Oriakhi, I. V. Farr, and M. M. Lerner, *J. Mater. Chem.* **6,** 103 (1996).
32. H. A. Thompson, G. A. Parks, and G. E. Brown Jr. *Clays Clay Miner.* **47,** 425 (1999).
33. W. Hofmeister and H. von Platen, *Cryst. Rev.* **3,** 3 (1992).
34. N Alberding and E. D. Crozier, *Phys. Rev. B* **27,** 3374 (1983).
35. P. Rabu, S. Angelov, P. Legoll, M. Belaiche, and M. Drillon, *Inorg. Chem.* **32,** 2463 (1993).
36. M. Drillon and P. Panissod, *J. Magn. Magn. Mater.* **188,** 93 (1998).
37. S. Angelov, M. Drillon, E. Zhecheva, R. Stoyanova, M. Belaiche, A. Derory, and A. Herr, *Inorg. Chem.* **31,** 1514 (1992).

38. M. Kurmoo, P. Day, A. Derory, C. Estournès, R. Poinsot, M. J. Stead, and C. J. Kepert, *J. Solid State Chem.* **145,** 452 (1999).
39. W. Fujita, K. Awaga, and T. Yokayama, *Appl. Clay Sci.* **15,** 281 (1999).
40. F. Sanz, C. Parada, J. M. Rojo, and C. Ruiz-Valero, *Chem. Mater.* **11,** 2673 (1999); J. M. Amarilla, R. M. Rojas, J. M. Rojo, M. J. Cubillo, A. Linares, and J. L. Acosta, *Solid State Ionics* **127,** 133 (2000).
41. J. Emery, J. Y. Buzare, O. Bohnke, and J. L. Fourquet, *Solid State Ionics* **99,** 41 (1997).
42. A. De Roy and J.-P. Besse, *Solid State Ionics* **46,** 95 (1991).
43. V. Ducos, A. de Roy, and J.-P. Besse, *Solid State Ionics* **145,** 399 (2001).
44. E. Ruiz-Hitzy, J. C. Galvan, J. Merino, B. Casal, P. Aranda, and A. Jimenez-Morales, *Solid State Ionics* **85,** 313 (1996).